Atomic force microscopy reveals the stoichiometry and subunit arrangement of 5-HT_3 receptors

Nelson P. Barrera*, Paul Herbert†, Robert M. Henderson*, Ian L. Martin†, and J. Michael Edwardson*‡

*Department of Pharmacology, University of Cambridge, Tennis Court Road, Cambridge CB2 1PD, United Kingdom; and †School of Life and Health Sciences, Aston University, Aston Triangle, Birmingham B4 7ET, United Kingdom

Edited by Arthur Karlin, Columbia University College of Physicians and Surgeons, New York, NY, and approved July 21, 2005 (received for review April 20, 2005)

The 5-HT_3 receptor is a cation-selective ligand-gated ion channel of the Cys-loop superfamily. The receptor is an important therapeutic target, with receptor antagonists being widely used as antiemetics in cancer therapy. The two known receptor subunits, A and B, form homomeric 5-HT_{3A} receptors and heteromeric 5-$HT_{3A/B}$ receptors. The heteromeric receptor has the higher single-channel conductance and more closely mimics the properties of the native receptor. We have used atomic force microscopy to study the architecture of 5-HT_{3A} and 5-$HT_{3A/B}$ receptors. We engineered different epitope tags onto the A- and B-subunits and imaged receptors that were doubly liganded by anti-epitope antibodies. We found that, for the 5-$HT_{3A/B}$ receptor, the distribution of angles between antibodies against the A-subunit had a single peak at ≈144°, whereas the distribution for antibodies against the B-subunit had two peaks at ≈72° and 144°. Our results indicate that the subunit stoichiometry is 2A:3B and that the subunit arrangement around the receptor rosette is B–B–A–B–A. This arrangement may account for the difference between the agonist Hill coefficients and the single-channel conductances for the two types of receptor.

ligand-gated ion channel | receptor structure

The 5-HT_3 receptor is a member of the Cys-loop ligand-gated ion channel superfamily, together with the nicotinic acetylcholine receptor, the $GABA_A$ receptor, and the glycine receptor (1–3). Electron microscopy of the affinity purified 5-HT_3 receptor has shown that it contains five subunits arranged pseudosymmetrically around a cylinder of long axis 11 nm and external diameter 8 nm (4, 5). The vestibule of the channel, normally open to the cell exterior, is visible as an opening of diameter 2–3 nm. Two 5-HT_3 receptor subunits have been investigated in detail. The first to be cloned, 5-HT_{3A} (6), expresses as a functional homomer, whereas the second, 5-HT_{3B}, is unable to form functional channels alone but expresses robustly in the presence of the 5-HT_{3A} subunit (7). The genes for these two subunits are located in close proximity on chromosome 11, although additional putative 5-HT_3 receptor genes have been isolated on chromosome 3 (8). The biophysical properties of the 5-HT_{3A} and the 5-$HT_{3A/B}$ receptors exhibit significant differences, with those of the heteromer more closely resembling those of the receptor characterized within the majority of mammalian systems (9–12). Competitive antagonists of 5-HT_3 receptors are used clinically as antiemetics in cancer chemotherapy and in general anesthesia, although other applications are being explored (13). The two receptor subtypes are difficult to distinguish pharmacologically (14), although picrotoxin (15) and tubocurarine (7) are markedly less potent in blocking agonist-induced currents in the exogenously expressed heteromeric receptors. Although there is some anatomical evidence that the homomeric receptor may be expressed alone in the rat (16, 17), current functional evidence suggests that it is the heteromer that is of major importance both centrally and in the periphery.

Despite its considerable physiological and therapeutic significance, the architecture of the 5-$HT_{3A/B}$ receptor is far from clear. Here, we have used atomic force microscopy (AFM) to image the heteromeric receptor, expressed after engineering distinct epitope tags onto the two subunits, and used the purified receptor from these preparations to elucidate the stoichiometry and arrangement of the A- and B-subunits within the heteromeric 5-$HT_{3A/B}$ receptor.

Materials and Methods

Transient Transfection of tsA 201 Cells. cDNA encoding the 5-HT_3 receptor A-subunit, with a C-terminal Myc/His-6 epitope tag, was subcloned into the vector pcDNA3.1 (Invitrogen) by using HindIII/XhoI. cDNA encoding the B-subunit, with a C-terminal V5/His-6 epitope tag, was subcloned into the same vector by using HindIII/BamHI. Transfections of tsA 201 cells (a subclone of HEK 293 cells stably expressing the SV40 large T-antigen) were carried out by using the CalPhos mammalian transfection kit (Clontech). After transfection, cells were incubated for 24–48 h at 37°C to allow expression of the receptors.

Solubilization and Purification of His-6-Tagged Receptors. The solubilization/purification procedure was done as described in ref. 18 for P2X receptors. Briefly, a crude membrane fraction prepared from transfected tsA 201 cells was solubilized in 1% (wt/vol) 3-[(3-cholamidopropyl)dimethylammonio]-1-propanesulfonate, and the solubilized material was incubated with Ni^{2+}-agarose beads (Probond, Invitrogen). The beads were washed extensively, and bound protein was eluted with increasing concentrations of imidazole. Samples were analyzed by SDS/PAGE, and protein was detected by immunoblotting. The receptor was detected by using mouse monoclonal antibodies (mAbs) against the His-6 tag on either subunit (Invitrogen; 1:500), the Myc tag on the A-subunit (Roche; 1:500), or the V5 tag on the B-subunit (Invitrogen; 1:500), as appropriate.

AFM Imaging of Receptors and Receptor–Antibody (Ab) Complexes. The 5-HT_3 receptors were imaged either alone or after incubation for 14 h at 4°C with a 1:2 molar ratio (≈0.2 nM receptor concentration) of one of the following mouse mAbs: anti-His-6 IgG (Research Diagnostics, Flanders, NJ) or anti-Myc for both 5-HT_{3A} and 5-$HT_{3A/B}$ receptors, and anti-V5 for the 5-$HT_{3A/B}$ receptor. The anti-V5 Ab also was incubated with the 5-HT_{3A} receptor as a negative control. Proteins were diluted to a final concentration of 0.04 nM, and 45 μl of the sample was allowed to adsorb to freshly cleaved, poly(L-lysine)-coated mica coverslips (Sigma). After a 10-min incubation, the sample was washed with MilliQ-water and dried under nitrogen. Imaging was performed with a Multimode atomic force microscope (Digital Instruments, Santa Barbara, CA). Samples were imaged in air, and experiments were carried out in tapping mode. The silicon cantilevers used had a drive frequency of ≈300 kHz

This paper was submitted directly (Track II) to the PNAS office.

Abbreviation: AFM, atomic force microscopy.

‡To whom correspondence should be addressed. E-mail: jme1000@cam.ac.uk.

and a specified spring constant of 40 N/m (MikroMasch, Portland, OR). The applied imaging force was kept as low as possible (target amplitude ≈ 1.6–1.8 V and amplitude setpoint ≈ 1.3–1.5 V).

The molecular volumes of the protein particles were determined from particle dimensions based on AFM images. After adsorption of the receptors onto the mica support, the particles adopt the shape of a spherical cap. The heights and half-height radii were measured from multiple cross-sections of the same particle, and the molecular volume was calculated by using the following equation:

$$V_m = (\pi h/6)(3r^2 + h^2), \quad [1]$$

where h is the particle height and r is the radius (19).

Molecular volume based on molecular mass was calculated by using the equation

$$V_c = (M_0/N_0)(V_1 + dV_2), \quad [2]$$

where M_0 is the molecular mass, N_0 is Avogadro's number, V_1 and V_2 are the partial specific volumes of particle and water, respectively, and d is the extent of protein hydration (19). The volume contributions of core protein and attached oligosaccharides were calculated by using previously reported values of partial specific volumes for protein (0.74 cm^3/g) and carbohydrate (0.61 cm^3/g) (20). For the extent of protein hydration, we used the value of 0.4 g of water per g of protein reported for a typical globular protein (human serum albumin) (21).

Results

The 5-HT_{3A} and 5-$HT_{3A/B}$ receptors were produced in tsA 201 cells by transfection with the appropriate cDNAs. The A-subunit bore a Myc/His-6 tag at its C terminus, whereas the B-subunit bore a V5/His-6 tag, also at its C terminus. In cells transfected with cDNAs for both A- and B-subunits (at a 1:1 ratio by weight), anti-His-6, anti-Myc, and anti-V5 Abs all gave positive immunofluorescence signals that were consistent with the presence of the majority of the 5-$HT_{3A/B}$ receptor at the plasma membrane (Fig. 1*A*). In cells transfected with cDNA for the A-subunit only, the anti-His-6 and anti-Myc Abs gave positive signals, but the anti-V5 Ab was negative, as expected. Both the 5-HT_{3A} receptor and the 5-$HT_{3A/B}$ receptor expressed in the tsA 201 cells showed very similar [^{3}H]granisetron binding characteristics to those reported elsewhere for untagged receptors (data not shown). In addition, it has been shown previously that very similar constructs produce 5-HT-triggered channel activity in both tsA 201 (22) and HEK 293 (7) cells. We are confident, therefore, that both forms of the receptor are functional.

Crude membrane fractions of the transfected cells were solubilized in the detergent 3-[(3-cholamidopropyl)dimethylammonio]-1-propanesulfonate, and the receptors were isolated through their binding to Ni^{2+}-agarose columns via their His-6 tags. As shown in Fig. 1*B*, the isolated 5-HT_{3A} receptor was not detected on immunoblots with the anti-V5 Ab but exhibited two bands at 50 and 55 kDa with the anti-Myc Ab. The mobility of the upper band is as expected of the glycosylated A-subunit (23); the lower band likely represents an incompletely glycosylated subunit (23). The 5-$HT_{3A/B}$ receptor differed only in the appearance of a 50-kDa band with the anti-V5 Ab.

The 5-HT_{3A} and 5-$HT_{3A/B}$ receptor preparations were adsorbed to a mica support, dried, and subjected to AFM imaging in air. In an initial control experiment, a sample from mock-transfected cells was imaged. As shown in Fig. 2*A*, this sample was almost featureless. In contrast, both 5-HT_{3A} and 5-$HT_{3A/B}$ receptor populations appeared as homogenous spreads of

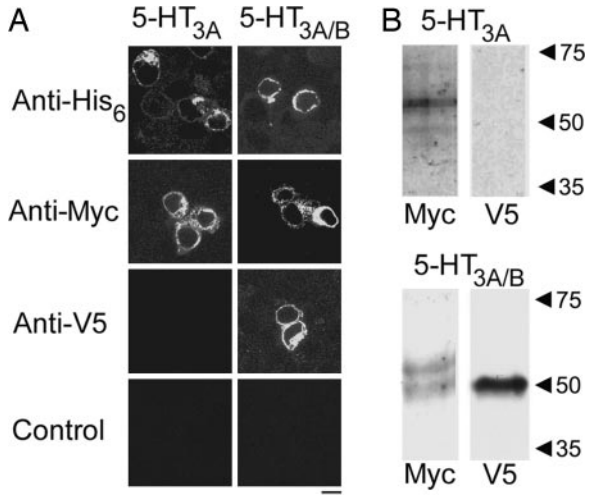

Fig. 1. Immunofluorescence and immunoblot analysis of 5-HT_3 receptors. (*A*) Immunofluorescence detection of 5-HT_3 receptors in transfected tsA 201 cells. Cells were fixed, permeabilized, and incubated with primary mAbs, followed by a Cy3-conjugated goat anti-mouse secondary Ab. In control incubations, the primary Ab was omitted. Cells were imaged by confocal laser scanning microscopy. (Scale bar, 10 μm.) (*B*) Detection of 5-HT_{3A} and 5-$HT_{3A/B}$ receptors in eluates from Ni^{2+}-agarose columns. Samples were analyzed by SDS/PAGE and immunoblotting, using monoclonal anti-Myc and anti-V5 primary Abs followed by a horseradish peroxidase-conjugated goat anti-mouse secondary Ab. Immunoreactive bands were visualized by using enhanced chemiluminescence.

particles (Fig. 2 *B–E*). The difference in the appearances of the samples from mock-transfected and transfected cells strongly indicates that the particles represent isolated receptors. The heights and radii of a number of receptor particles from each sample were determined as indicated in Fig. 2 *F–I*. Particle radii were measured at half the maximal height to compensate for the tendency of AFM to overestimate this parameter when the radii of both particle and scanning tip are similar (i.e., in the nanometer range). By using this method, a very good correlation was obtained previously between predicted and calculated molecular volumes for proteins of widely varying molecular masses (19). The particle dimensions measured indicate a flattening, caused principally by the spreading of the proteins on the polar mica surface, as described in refs. 18 and 24. The dimensions were used to calculate molecular volumes by using Eq. **1**. The frequency distributions of the calculated molecular volumes are shown in Fig. 2 *J* and *K*. The histograms were fitted to a Gaussian function by using nonlinear regression. No differences between peak and mean values were obtained in either case ($P > 0.05$). The mean values of the molecular volumes (±SE) were 757 ± 31 nm^3 ($n = 149$) for the 5-HT_{3A} receptor and 704 ± 33 nm^3 ($n = 144$) for the 5-$HT_{3A/B}$ receptor. Assuming a subunit molecular mass of 55 kDa for the 5-HT_{3A} receptor, a pentameric receptor would have a total molecular mass of 275 kDa, of which ≈50 kDa is accounted for by attached oligosaccharides (23). The expected molecular volume, calculated from Eq. **2**, is 511 nm^3; hence, the molecular volume determined for the 5-HT_{3A} receptor was 48% greater than expected. The discrepancy between the predicted and measured values of molecular volume is likely caused by the presence of bound detergent and was observed previously during AFM imaging of the $GABA_A$ receptor (24). A similar overestimation (42%) also was found when native, purified 5-HT_3 receptors, solubilized in dodecylmaltoside, were sized by using gel filtration (4). The 5-$HT_{3A/B}$ receptor, with ≥1 copy of the smaller B-subunit, should be smaller than the 5-HT_{3A} receptor; however, the difference between the observed mo-

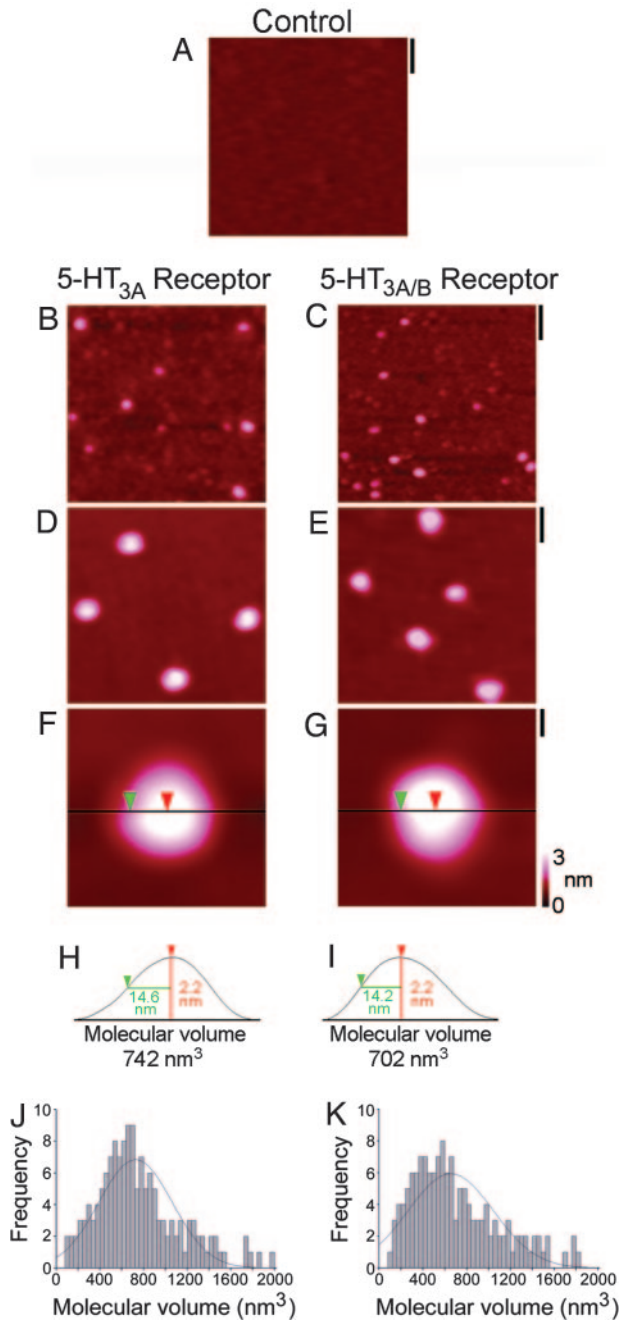

Fig. 2. AFM imaging of 5-HT_{3A} and 5-$HT_{3A/B}$ receptors. (*A*) Low-magnification image of a sample prepared from mock-transfected cells. (Scale bar, 100 nm.) (*B* and *C*) Low-magnification images of 5-HT_{3A} (*B*) and 5-$HT_{3A/B}$ (*C*) receptors. (Scale bar, 100 nm.) (*D* and *E*) Medium-magnification images. (Scale bar, 50 nm.) (*F* and *G*) High-magnification images of single 5-HT_{3A} (*F*) and 5-$HT_{3A/B}$ (*G*) receptors. (Scale bar, 10 nm.) A color-height scale is shown at the right. (*H* and *I*) Sections through the receptors shown in *F* and *G* at the positions indicated by the lines. The height of the receptors and their radii at half height are shown. (*J* and *K*) Frequency distributions of molecular volumes of 5-HT_{3A} (*J*) and 5-$HT_{3A/B}$ (*K*) receptors. The curves indicate fitted Gaussian functions.

lecular volumes of the two receptors was not statistically significant ($P > 0.05$).

The 5-HT_{3A} receptor was next imaged after incubation with mouse mAbs against either its His-6 or Myc tags. Images of the receptor alone and the Abs (IgG, molecular mass 150 kDa) alone are shown in Fig. 3 *A Left* and *Center* and *B Left* and

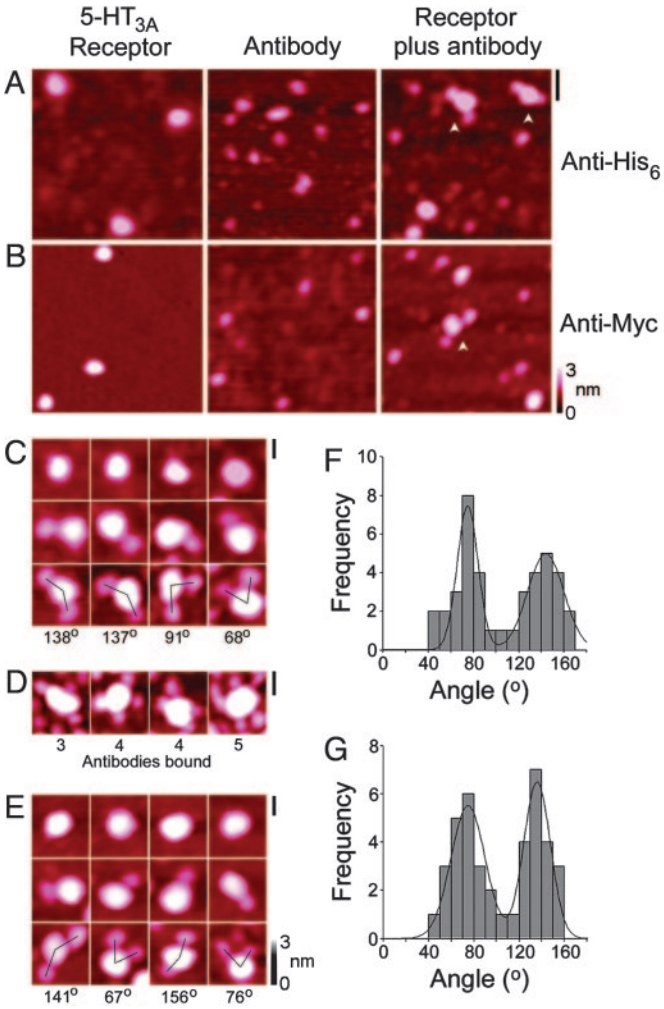

Fig. 3. AFM imaging of complexes between 5-HT_{3A} receptors and anti-His-6 and anti-Myc Abs. (*A* and *B*) Images of receptors (*Left*), Abs (*Center*), and receptor–Ab complexes (*Right*). (Scale bar, 50 nm.) (*C*) Zoomed images of receptors that are uncomplexed (*Top*) or bound by one (*Middle*) or two (*Bottom*) anti-His-6 Abs. (*D*) Zoomed images of receptors bound by three to five anti-His-6 Abs. (*E*) Zoomed images of receptors that are uncomplexed (*Top*) or bound by one (*Middle*) or two (*Bottom*) anti-Myc Abs. (Scale bars: *C–E*, 20 nm.) (*F* and *G*) Frequency distributions of angles between anti-His-6 (*F*) or anti-Myc (*G*) Abs.

Center. Both the receptor and the Abs appeared as homogenous populations of particles, and the Abs were clearly smaller than the receptors. When the suspensions resulting from the receptor–Ab coincubations were imaged, various structures were seen (Fig. 3 *A Right* and *B Right*), including large and small particles, representing receptors and Abs, and receptor–Ab complexes (arrowheads). When the receptor was incubated with either the anti-His-6 Ab or the anti-Myc Ab, the majority of the receptors were uncomplexed, but a significant minority had either one or two Abs bound (Table 1). When receptors were imaged alone, or after incubation with the anti-V5 Ab, only a small percentage of the receptors appeared to be associated with bound particles. These particles presumably represent structures that happened to attach to the mica alongside receptors. These data indicate that the vast majority of the binding events observed with the anti-His-6 or anti-Myc Abs represent specific receptor–Ab interactions.

The distribution of the various Ab-binding states observed deviates from that predicted by the binomial distribution,

Table 1. Antibody tagging profile of the 5-HT$_3$ receptors

No. of particles bound to receptor	Receptor alone, no. (%)	Receptor plus anti-His$_6$ Ab, no. (%)	Receptor plus anti-Myc Ab, no. (%)	Receptor plus anti-V5 Ab, no. (%)
5-HT$_{3A}$ receptor				
0	149 (97.4)	331 (69.7)	238 (63.0)	156 (97.5)
1	4 (2.6)	98 (20.6)	95 (25.1)	4 (2.5)
2	0 (0.0)	40 (8.4)	40 (10.6)	0 (0.0)
3	0 (0.0)	1 (0.2)	4 (1.0)	0 (0.0)
4	0 (0.0)	4 (0.9)	1 (0.3)	0 (0.0)
5	0 (0.0)	1 (0.2)	0 (0.0)	0 (0.0)
5-HT$_{3A/B}$ receptor				
0	144 (98.0)	372 (72.0)	220 (62.5)	187 (58.8)
1	3 (2.0)	101 (19.5)	92 (26.1)	87 (27.3)
2	0 (0.0)	40 (7.7)	40 (11.4)	40 (12.6)
3	0 (0.0)	3 (0.6)	0 (0.0)	4 (1.3)
4	0 (0.0)	1 (0.2)	0 (0.0)	0 (0.0)
5	0 (0.0)	0 (0.0)	0 (0.0)	0 (0.0)

which should apply here, assuming that there is a fixed probability of Ab binding to its epitopes on the subunits. Specifically, the higher binding states are overrepresented. One possible explanation for this discrepancy, which is similar for all three Abs used, is that the various receptor–Ab complexes do not attach to the mica with equal probabilities. For instance, it is likely that the presence of a bound Ab would increase the electrostatic attraction between the particle and the poly(L-lysine)-coated mica surface, thereby increasing the probability that multiply complexed receptors will attach.

Fig. 3*C* shows a gallery of images of receptors with zero, one, and two bound anti-His-6 Abs. Very occasionally, receptors bound by three to five Abs also were seen (Fig. 3*D*). Hence, it is possible to occupy all five A-subunits with Abs, although the chances of complete occupation are small. Similar features were apparent when the anti-Myc Ab was used (Fig. 3*E*). For doubly complexed receptors (Fig. 3 *C* and *E*), the angles between the pairs of bound Abs were calculated by joining the height peaks of the Ab particles to the height peak of the receptor particle. The angles were used to construct the frequency distributions shown in Fig. 3 *F* and *G*. For both anti-His-6 and anti-Myc Abs, the distributions had two clear peaks. The means of the two distributions are 72 ± 3° (n = 21) and 144 ± 3° (n = 19) for the anti-His-6 Ab and 73 ± 3° (n = 20) and 136 ± 3° (n = 20) for the anti-Myc Ab. These data indicate that the Ab-bound subunits were either adjacent (expected angle 72°) or separated by another subunit (expected angle 144°). Note also that for both Abs, the heights of the two peaks were approximately equal, indicating that there was no steric effect hindering the binding of two Abs to adjacent subunits.

The same series of experiments was carried out for the 5-HT$_{3A/B}$ receptor, except using the anti-V5 Ab in addition to the anti-His-6 and the anti-Myc Abs. The numbers of receptors in the various binding states under the different conditions used are shown in Table 1. As for the 5-HT$_{3A}$ receptor, the data indicate a specific binding of the 5-HT$_{3A/B}$ receptor by anti-His-6, anti-Myc and anti-V5 Abs. Note that, in contrast to anti-His-6 Ab binding, no 5-HT$_{3A/B}$ receptor was bound by more than two anti-Myc Abs or more than three anti-V5 Abs. Fig. 4 *A–C* shows galleries of images of receptors with zero, one, and two bound Abs for anti-His-6, anti-Myc, and anti-V5, respectively. Corresponding frequency distributions of the angles between pairs of bound Abs are shown in Fig. 4 *D–F*. The distributions of the anti-His-6 and the anti-V5 receptor Abs had two peaks, with means of 73 ± 3° (n = 15) and 145 ± 2° (n = 25) for the anti-His-6 Ab and 74 ± 3° (n = 18) and 140 ± 3° (n = 22) for the anti-V5 Ab. In contrast, the distribution for the anti-Myc Ab had a single peak, and the mean of the distribution was 140 ± 3° (n = 40). These results indicate the following: (*i*) that both A- and B-subunits are present in the 5-HT$_{3A/B}$ receptor in more than one copy; (*ii*) that the B-subunits, bearing V5 tags, can be either adjacent or separated by another subunit, and (*iii*) that the A-subunits, bearing Myc tags, are always separated by another subunit. The only subunit stoichiometry that is consistent with these data is 2A:3B, and the only possible arrangement of subunits around the receptor rosette is B–B–A–B–A. The gallery of zoomed images in Fig. 4*G* shows receptors that are doubly complexed with anti-Myc Abs (at an obtuse angle) or by anti-V5 Abs (at either an acute or an obtuse angle). A composite of these three images (Fig. 4*H*) illustrates the B–B–A–B–A subunit arrangement.

Discussion

Our data indicate that the 5-HT$_{3A/B}$ receptor adopts a single subunit configuration when expressed in tsA 201 cells. This result was expected, given what we know about the heteromeric 5-HT$_3$ receptor and other Cys-loop receptors. For instance, a single conductance state is observed when the A- and B-subunits are coexpressed (7, 22), suggesting that the two subunits assemble to produce a single type of heteromeric receptor. The *Torpedo* electroplaque nicotinic acetylcholine receptor, too, has a unique subunit arrangement, α, γ, α, δ, β, when viewed counterclockwise from the outside of the cell (1, 2). Further, when the GABA$_A$ receptor produced by coexpression of α_1, β_2, and γ_2 subunits was analyzed, there was again evidence for a single subunit stoichiometry, 2α:2β:1γ (25). Additionally, study of the functional properties of different combinations of concatenated subunits has indicated a unique subunit arrangement, γ_2, β_2, α_1, β_2, α_1, when viewed counterclockwise from the outside of the cell (26). It seems, therefore, that a unique assembly pattern occurs when a cell is provided with a combination of subunits for a particular ionotropic receptor, and this situation seems to prevail in our studies.

The ring-like immunofluorescence images indicate that most of the 5-HT$_3$ receptors are expressed at the plasma membrane; however, there is also likely to be an intracellular pool. Further, the immunoblots reveal that not all of the A-subunit is glycosylated, whereas the B-subunit appears to exist in a single glycosylated state. The possibility that these

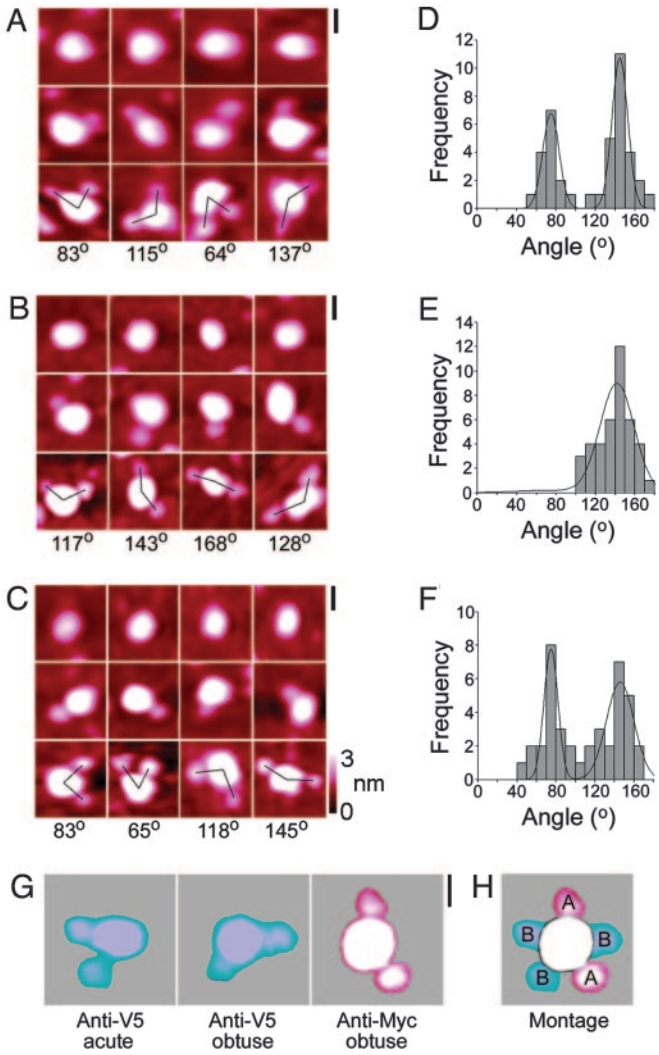

Fig. 4. AFM imaging of complexes between 5-$HT_{3A/B}$ receptors and anti-His-6, anti-Myc, and anti-V5 Abs. (*A–C*) Zoomed images of receptors that are either uncomplexed (*Top*), or bound by one (*Middle*) or two (*Bottom*) anti-His-6 (*A*), anti-Myc (*B*), or anti-V5 (*C*) Abs. (*D–F*) Frequency distributions of angles between Abs for receptors doubly bound by anti-His-6 (*D*), anti-Myc (*E*), or anti-V5 (*F*) Abs. (*G*) Zoomed images of receptors that are doubly bound by either anti-V5 or anti-Myc Abs. (*H*) Composite of the three images shown in *G* illustrating the B–B–A–B–A arrangement of subunits around the receptor rosette. (All scale bars, 20 nm.)

complications might affect the outcome of our experiments should be considered. There is good evidence that assembly of other Cys-loop receptors, such as the nicotinic (27) and $GABA_A$ (28) receptors, occurs in the endoplasmic reticulum soon after polypeptide synthesis. It is therefore likely that even receptors that have not arrived at the plasma membrane are correctly assembled. The significance of glycosylation with respect to the stability and characteristics of the 5-HT_{3A} receptor homomer has been investigated (23). It was found that inhibition of glycosylation by tunicamycin resulted in a significant reduction in [^{3}H]granisetron binding and a retention of the receptor in the endoplasmic reticulum. How the concomitant presence of the B-subunit in our experiments will affect the behavior of the unglycosylated fraction of the A-subunit is not clear. However, we would emphasize that there is no evidence from our data for the existence of more than one population of receptors.

The subunit arrangement that we propose for the 5-$HT_{3A/B}$ receptor allows us to rationalize two functional characteristics of the receptor, the 40-fold difference between the single-channel conductances of the homomeric and heteromeric receptors and the difference between the Hill coefficents for agonist action at the two types of receptor. Interestingly, mutations in the 5-HT_{3A} subunit, within a putative intracellular amphipathic helix identified in the nicotinic acetylcholine receptor (29, 30), in which three nonsequential arginine residues are replaced by the equivalent residues from the 5-HT_{3B} subunit, yield a receptor with a single-channel conductance of 22 pS, larger than that of the wild-type (WT) 5-$HT_{3A/B}$ receptor (13 pS) (22). It is argued that in the 5-HT_{3A} receptor the charge on these arginine residues compromises the exit of permeant ions from the channel to the intracellular environment. Further, when this mutant is expressed together with the WT 5-HT_{3A} subunit, the channel conductance is almost identical to that found in the WT heteromeric 5-$HT_{3A/B}$ receptor. Because these intracellular ion exits are found at the subunit interfaces, the B–B–A–B–A arrangement that we suggest numerically reflects the contributions of the subunits to channel conductance in the WT heteromer.

The proposed subunit arrangement also may account for the observation that the Hill coefficient for agonist activation is significantly lower in the 5-$HT_{3A/B}$ receptor than in the 5-HT_{3A} receptor (7, 31). The agonist recognition sites are found at interfaces between the extracellular domains of the subunits (32). In the homomer, there will be five A–A subunit interfaces and, thus, five structurally equivalent sites, whereas in the heteromer there will be three types of subunit interface, 2 × A–B, 2 × B–A, and 1 × B–B. The fact that the Hill coefficient for the agonist activation of the heteromer is about half that of the homomer (33) indicates that these different interfaces provide nonequivalent agonist-binding sites. The crystal structure of the acetylcholine binding protein (34) has been used as a template to refine the structural models of the nicotinic acetylcholine receptor (30, 35) where the subunit stoichiometry (36) and arrangement (37) are known. It should now be possible, with the information presented here, to extend this analysis to the heteromeric 5-$HT_{3A/B}$ receptor, to characterize the potential agonist binding sites.

In light of the fact that the B-subunit by itself cannot assemble to form ligand-binding complexes and cannot exit the endoplasmic reticulum in transfected cells (33), the presence of a B–B subunit interface in the 5-$HT_{3A/B}$ heteromer, as proposed here, is interesting. It is known that the assembly of the electroplaque nicotinic receptor proceeds through the formation of trimers and tetramers and that subunit folding requires the presence of particular subunit combinations (38). It is possible, therefore, that the correct folding and subsequent assembly of the B-subunits in the endoplasmic reticulum requires the concomitant presence of A-subunits.

We have now used AFM imaging of Ab-decorated receptors to provide information about the architecture of three types of ligand-gated ion channel, the $GABA_A$ (24), the P2X (18), and the 5-HT_3 receptors. We suggest that the method that we describe here can be applied not only to other members of the ligand-gated ion channel superfamilies (1–3, 39) but also more widely to other types of multisubunit protein.

We thank M. Davies (Department of Pharmacology, University of Alberta, Edmonton, Canada) for providing the 5-HT_3 receptor cDNA constructs and N. M. Barnes for advice on the immunoblotting with the anti-Myc Ab. This work was supported by Biotechnology and Biological Sciences Research Council Grant B19797 (to J.M.E. and R.M.H.) and, in part, by Wellcome Trust Grant 069380 (to I.L.M. and S. M. J. Dunn) and the Canadian Institutes of Health Research (to S. M. J. Dunn and I.L.M.).

1. Corringer, P.-J., Le Novère, N. & Changeux, J.-P. (2000) *Annu. Rev. Pharmacol. Toxicol.* **40,** 431–458.
2. Karlin, A. (2002) *Nat. Rev. Neurosci.* **3,** 102–114.
3. Lester, H. A., Dibas, M. I., Dahan, D. S., Leite, J. F. & Dougherty, D. A. (2004) *Trends Neurosci.* **27,** 329–336.
4. Boess, F. G., Lummis, S. C. R. & Martin, I. L. (1992) *J. Neurochem.* **59,** 1692–1701.
5. Boess, F. G., Beroukhim, R. & Martin, I. L. (1995) *J. Neurochem.* **64,** 1401–1405.
6. Maricq, A. V., Peterson, A. S., Brake, A. J., Myers, R. M. & Julius, D. (1991) *Science* **254,** 432–437.
7. Davies, P. A., Pistis, M., Hanna, M. C., Peters, J. A., Lambert, J. J., Hales, T. G. & Kirkness, E. F. (1999) *Nature* **397,** 359–363.
8. Niesler, B., Frank, B., Kapeller, J. & Rappold, G. A. (2003) *Gene* **310,** 101–111.
9. Derkach, V., Surprenant, A. & North, R. A. (1989) *Nature* **339,** 706–709.
10. Yang, J., Mathie, A. & Hille, B. (1992) *J. Physiol.* **448,** 237–256.
11. Hussy, N., Lukas, W. & Jones, K. A. (1994) *J. Physiol.* **481,** 311–323.
12. Jones, K. A. & Surprenant, A. (1994) *Neurosci. Lett.* **174,** 133–136.
13. Jones, B. J. & Blackburn, T. P. (2002) *Pharmacol. Biochem. Behav.* **71,** 555–568.
14. Brady, C. A., Stanford, I. M., Ali, I., Lin, L., Williams, J. M., Dubin, A. E., Hope, A. G. & Barnes, N. M. (2001) *Neuropharmacology* **41,** 282–284.
15. Das, P. & Dillon, G. H. (2003) *Brain Res. Mol. Brain Res.* **119,** 207–212.
16. Morales, M., McCollum, N. & Kirkness, E. F. (2001) *J. Comp. Neurol.* **438,** 163–172.
17. Morales, M. & Wang, S.-D. (2002) *J. Neurosci.* **22,** 6732–6741.
18. Barrera, N. P., Ormond, S. J., Henderson, R. M., Murrell-Lagnado, R. D. & Edwardson, J. M. (2005) *J. Biol. Chem.* **280,** 10759–10765.
19. Schneider, S. W., Lärmer, J., Henderson, R. M. & Oberleithner, H. (1998) *Pflügers Arch.* **435,** 362–367.
20. Durchschlag, H. & Zipper, P. (1997) *J. Appl. Crystallogr.* **30,** 803–807.
21. Grant, E. H. (1957) *Phys. Med. Biol.* **2,** 17–28.
22. Kelley, S. P., Dunlop, J. I., Kirkness, E. F., Lambert, J. J. & Peters, J. A. (2003) *Nature* **424,** 321–324.
23. Monk, S. A., Williams, J. M., Hope, A. G. & Barnes, N. M. (2004) *Biochem. Pharmacol.* **68,** 1787–1796.
24. Neish, C. S., Martin, I. L., Davies, M., Henderson, R. M. & Edwardson, J. M. (2003) *Nanotechnology* **14,** 864–872.
25. Farrar, S. J., Whiting, P. J., Bonnert, T. P. & McKernan, R. M. (1999) *J. Biol. Chem.* **274,** 10100–10104.
26. Baumann, S., Baur, R. & Sigel, E. (2002) *J. Biol. Chem.* **277,** 46020–46025.
27. Smith, M. M., Lindstrom, J. & Merlie, J. P. (1987) *J. Biol. Chem.* **262,** 4367–4376.
28. Connolly, C. N., Krishek, B. J., McDonald, B. J., Smart, T. G. & Moss, S. J. (1996) *J. Biol. Chem.* **271,** 89–96.
29. Miyazawa, A., Fujiyoshi, Y, Stowell, M. & Unwin, N. (1999) *J. Mol. Biol.* **288,** 765–786.
30. Unwin, N. (2005) *J. Mol. Biol.* **346,** 967–989.
31. Dubin, A. E., Huvar, R., D'Andrea, M. R., Pyati, J., Zhu, J. Y., Joy, K. C., Wilson, S. J., Galindo, J. E., Glass, C. A., Luo, L., *et al.* (1999) *J. Biol. Chem.* **274,** 30799–30810.
32. Reeves, D. C., Sayed, M. F. R., Chau, P.-L., Price, K. L. & Lummis, S. C. R. (2003) *Biophys. J.* **84,** 2338–2344.
33. Boyd, G. W., Low, P., Dunlop, J. I., Roberston, L. A., Vardy, A., Lambert, J. J., Peters, J. A. & Connolly, C. N. (2002) *Mol. Cell. Neurosci.* **21,** 38–50.
34. Brejc, K., van Dijk, W. J., Klaassen, R. V., Schuurmans, M., van Der Oost, J., Smit, A. B. & Sixma, T. K. (2001) *Nature* **411,** 269–276.
35. Celie, P. H., van Rossum-Fikkert, S. E., van Dijk, W. J., Brejc, K., Smit, A. B. & Sixma, T. K. (2004) *Neuron* **41,** 907–914.
36. Reynolds, J. A. & Karlin, A. (1978) *Biochemistry* **17,** 2035–2038.
37. Karlin, A., Holtzman, E., Yodh, N., Lobel, P., Wall, J. & Hainfeld, J. (1983) *J. Biol. Chem.* **258,** 6678–6681.
38. Green, W. N. & Claudio, T. (1993) *Cell* **74,** 57–69.
39. Le Novère, N. & Changeux, J.-P. (1999) *Nucleic Acids Res.* **27,** 340–342.